Index-symmetry breaking of polarization vortices in 2D random vector waves

de Angelis, L.; Bauer, T.; Alpeggiani, F.; Kuipers, L.

DOI
10.1364/OPTICA.6.001237

Publication date
2019

Document Version
Final published version

Published in
Optica

Research Article Vol. 6, No. 9 / September 2019 / Optica 1237

Index-symmetry breaking of polarization vortices in 2D random vector waves

L. De Angelis,[1,2] T. Bauer,[1] F. Alpeggiani,[1] and L. Kuipers[1,*]

[1]Kavli Institute of Nanoscience, Delft University of Technology, 2600 GA, Delft, The Netherlands
[2]The Netherlands Institute for Neuroscience, Institute of the Royal Netherlands Academy of Arts and Sciences (KNAW), Amsterdam, The Netherlands
*Corresponding author: l.kuipers@tudelft.nl

Received 16 May 2019; accepted 9 August 2019 (Doc. ID 367813); published 17 September 2019

When the positions of two generic singularities of equally signed topological index coincide, a higher-order singularity with twice the index is created. In general, singularities tend to repel each other when sharing the same topological index, preventing the creation of such higher-order singularities in 3D generic electromagnetic fields. Here, we demonstrate that in 2D random vector waves higher-order polarization singularities—known as polarization vortices—can occur, and we present their spatial correlation. These polarization vortices arise from the overlap of two points of circular polarization (C points) with the same topological index. We observe that polarization vortices of positive index occur more frequently than their negative counterparts, which results in an index-symmetry breaking unprecedented in singular optics. To corroborate our findings, we analyze the spatial correlation of C points in relation to their line classification and link the symmetry breaking to the allowed dipolar and quadrupolar moments of the field at a polarization vortex.

https://doi.org/10.1364/OPTICA.6.001237

1. INTRODUCTION

A hurricane generated from storms swirling in the ocean [1] and a peak in the gravitational-wave strain from the merging of two black holes [2] both represent observations of events in nature exhibiting singular parameters in their describing mathematical model. In many cases, these extreme events contain the formation or annihilation of vortices, given by a flow of a physical quantity around a singular point. Besides vortices present in systems with non-zero rest mass, they also exist in massless systems, such as light in the form of phase and polarization vortices [3–6]. While the former are the generic, lowest-order form of phase singularities, the latter represent higher-order polarization singularities. These are generated by the merging of two generic polarization singularities, namely two points of circular polarization (C points), where both singularities have the same topological index [7]. Polarization vortices are as a result exceptional points of the vector field that describes light. With the current knowledge and technology, light fields can be engineered to exhibit such higher-order singularities, typically on the optical axis of vortex beams of arbitrary angular momentum [8–12], or in radially and azimuthally polarized beams [13–19]. Contrarily, higher-order singularities are not to be expected in random ensembles of waves in 3D. In these fields, a multitude of lowest-order singularities occurs [20–22], but with a spatial repulsion between the ones with the same topological index [23–26]. However, a different physics governs the behavior of polarization singularities in 2D random light. In this case, the vicinity of same-index C points is promoted with respect to opposite-index ones [27], suggesting that despite their non-generic nature, polarization vortices might be abundant in these 2D fields.

In this paper, we report our observation of polarization vortices in 2D random vector waves. Besides their statistical emergence, we demonstrate that these higher-order singularities obey strict spatial correlation rules. Most surprisingly, the amount of polarization vortices occurring is not symmetric with respect to their topological index. An excess of positive vortices is found with respect to negative ones. This index imbalance concerns the ensemble of polarization vortices only, as considering all polarization singularities of the field together will still lead to index neutrality. We trace back our finding to the correlation of pairs of same-index C points in random light. We employ a vectorial model for 2D random fields to underpin the index imbalance as a consequence of the dimension of the vector field, which is truly two-dimensional. Finally, we explain this finding by attributing the field distribution around the vortices to the field's dipolar and quadrupolar moments.

2. EXPERIMENTAL OBSERVATION OF POLARIZATION VORTICES

We experimentally investigate polarization vortices in a two-dimensional random light field with a home-made polarization- and phase-resolving near-field microscope [28]. This allows us to map the in-plane optical field generated by the random interference of TE waves in a chaotic cavity [25,27,29]. The chaotic cavity [Fig. 1(a)] consists of a silicon-on-insulator photonic crystal cavity (220 nm thick layer of silicon on a silica buffer).

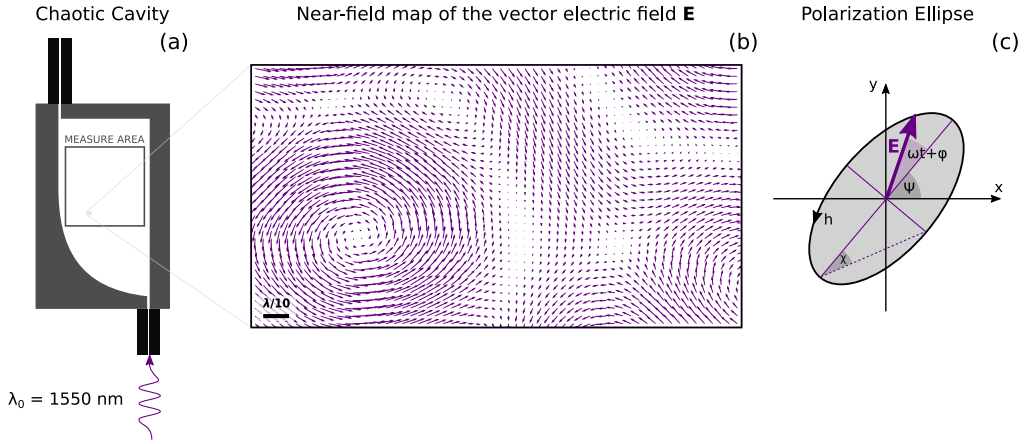

Fig. 1. Sketch of the experimental procedure. (a) Schematic of the chaotic cavity used for the generation of an optical random wave field. The gray area is a photonic crystal, confining TE light in the inner region of the cavity. The black areas constitute ridge waveguides for in-coupling and output. (b) Near-field measurement of the instantaneous electric field in the cavity. The purple arrows illustrate amplitude (length) and orientation (angle) of the TE electric field in the cavity, for $t = 0$. (c) Schematic of the polarization ellipse and its parameterization with orientation angle ψ, ellipticity angle χ, and handedness h.

In such a D-shaped arena, we generate an ensemble of random waves by injecting monochromatic light through an input waveguide [25]. With our aperture-based near-field probe we raster scan the surface of the cavity, specifically on the square region highlighted in Fig. 1(a). An interferometric detection approach [28,30] allows us to determine both amplitude and phase of each vector component of the in-plane TE field, with sub-wavelength resolution [25]. With this information, we can fully identify the polarization state of light at each experimental pixel. Figure 1(b) illustrates a zoomed-in section of a measurement, in which we employ our data to compute the instantaneous orientation (angle of arrows) and amplitude (length of arrows) of the electric field $\mathbf{E}(t)$ in the chaotic cavity. In general, the time evolution of these vectors describes an ellipse, sketched in Fig. 1(c) and known as the polarization ellipse.

When the polarization ellipse degenerates into a perfect circle, its orientation ψ becomes undetermined, generating a singularity in the director field, i.e., the field describing the orientation of the ellipse. These dislocations occur in general as points in a plane and are known as C points [31]. Here, we shift our attention from C points to higher-order singularities, consisting of two superimposed C points that share the same topological index. The topological index, or charge, of a polarization singularity is defined as

$$I = \frac{1}{2\pi}\int_{\mathcal{C}} \mathrm{d}\psi, \tag{1}$$

where ψ is the orientation angle of the local polarization ellipse and $\mathcal{C}$ is a closed path around the singularity. In this formalism, the detection of a polarization vortex is equivalent to that of lowest-order singularities, except that a double index is observed (see Appendix A for more details on the experimental approach).

With a pixel size of 17 nm in the experimental measurements, we detect approximately 80 polarization vortices per measured field map (17 μm × 17 μm) at a wavelength of $\lambda_{\mathrm{TE}} \approx 550$ nm (corresponding to a free-space wavelength of 1550 nm). This number is roughly 2 orders of magnitude smaller than the number of C points found in the same field map (≈6500), as is expected due to their higher-order nature. Note that dealing with experimental data with finite resolution we have to set an effective threshold below which two same-index C points are considered as one single polarization vortex. In a pragmatic way, we set this distance to be the pixel size of our experiment.

Figure 2 presents an illustrating set of four polarization vortices detected in one measured random field. Depending on their topological index (±1), the polarization vortices exhibit different topologies [32]. These differ from the three classes noted for C points, i.e., stars, lemons, and monstars [33,34]. Considering the orientation of the major axis of the polarization ellipse around the vortices (insets in Fig. 2), we identify two possibilities. For positive vortices ($I = +1$) the axes of the surrounding ellipses never point toward the singularity, resulting in a circular pattern around the vortex. In the case of negative vortices ($I = -1$) these directors point toward the singularity along four directions, forming a four-pointed star.

3. SPATIAL DISTRIBUTION OF POLARIZATION VORTICES

A. Pair and Charge Correlation Function and Index-Symmetry Breaking

While these singularities might appear to be the result of a seemingly arbitrary threshold, a distinct spatial correlation resulting from an underlying mechanism that governs their behavior would highlight their collective contribution to the general topology of random light fields. To characterize the spatial correlation of polarization vortices, we compute their pair and charge correlation functions $g(r)$ and $g_I(r)$. These functions are commonly used to describe the spatial distribution of point-like singularities [20], and of discrete systems of various types [35]. The $g(r)$ describes the spatial density variations of polarization vortices as a function of distance from each other. In the $g_I(r)$, each vortex is weighted additionally with its topological index. Because a single measurement frame contains only ∼80 vortices, we combine the outcome of 150 different measurements of the random light field. Thus, we achieve sufficiently good statistics for an experimental determination of $g(r)$ and $g_I(r)$.

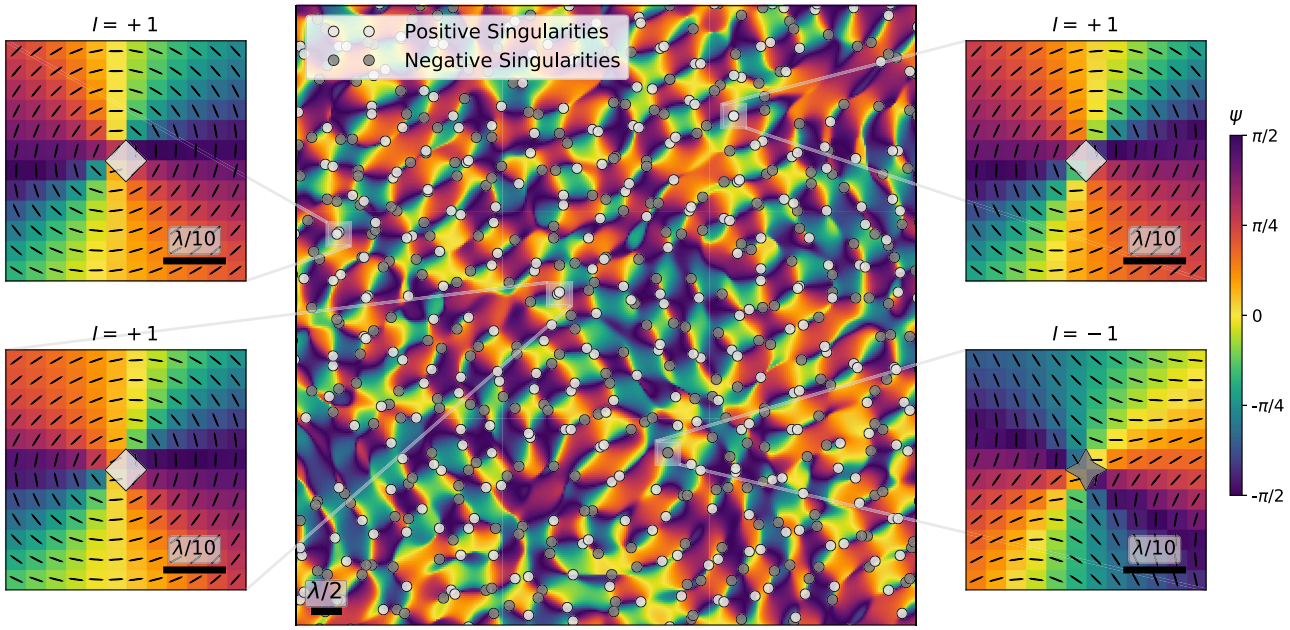

Fig. 2. False-color map for the orientation ψ of the major axis of the polarization ellipse in a 2D random light field (main plot). The plot is a 8.5 μm × 8.5 μm subsection of one measured field map. Markers correspond to C points. The color of the markers, light or dark gray, denotes a topological index of $+1/2$ or $-1/2$, respectively. In the observed map, four polarization vortices are highlighted (zoomed-in figures in the panels next to the main plot, with the major axis of the polarization ellipse additionally shown as black directors). These are depicted by light (index $+1$) or dark (index -1) gray symbols.

We find that the polarization vortices indeed exhibit a clear spatial correlation. Figure 3 presents the pair and charge correlation function for polarization vortices in 2D random vector waves. In these correlation functions we can identify several characteristic features. First, $g(r)$ clearly tends to zero when $r \approx 0$, indicating that polarization vortices are never to be found in close proximity regardless of their mutual sign, unlike C points. Second, the oscillation of this correlation function exhibits a much clearer contrast compared to the one displayed by C points [27] and phase singularities [25]. The first peak reaches values ≥ 4, more than twice as high as the values observed in the pair correlation function for C points. Additionally, this first peak in the $g(r)$ actually consists of two peaks. Interestingly, in the displacement range contained within the double peak of the $g(r)$, the $g_I(r)$ exhibits a zero crossing, going approximately from -4 to 2.5 over a distance of less than one fifth of light's wavelength. The average nearest-neighbor distance for pairs of same-sign vortices is 20% larger than that of opposite-sign vortices.

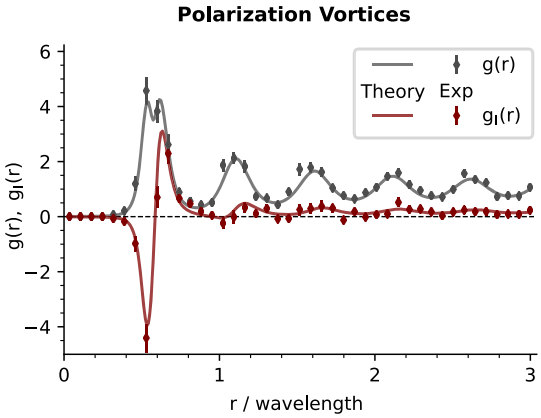

Fig. 3. Pair (g) and charge (g_I) correlation function for polarization vortices in random waves. The data points are representative of the experimental results, while solid lines are the result of the theory for polarization vortices in 2D random light.

Surprisingly, as r increases, $g_I(r)$ does not display a damped oscillatory behavior around zero but rather approaches a finite positive value. This indicates that index neutrality seems to be violated (see Appendix B). By counting the number of positive and negative vortices in a total of 150 measurements, we find an average ratio of vortices $f = N_+/N_- = 2.3 \pm 0.2$ for $N = 81.9 \pm 6.9$ vortices per measured field map. Such a strong imbalance in a topological index is highly unusual to find outside of elementary particle physics [36], and to our knowledge has not been observed so far for any other type of singularity in electromagnetic waves. This is corroborated by the fact that statistical properties of dislocations with opposite topological index are usually indistinguishable [33]. To understand the origin of this topological index asymmetry it is therefore useful to take one step back and reconsider the entities from which polarization vortices are formed: pairs of C points.

B. Index-Symmetry Breaking in the Spatial Distribution of C Points

Figure 4(a) presents the pair correlation function of C points for the cases in which both the singularities that constitute the pair have either positive (g^A_{++}, orange data) or negative (g^A_{--}, purple data) topological index, and reside in areas of opposite handedness of circular polarization (symbolized by the superscript A). The restriction to anti-handed C points as origin for polarization vortices is here given by the vanishing correlation function $g^C_{\text{same}}(r)$ for co-handed C points as $r \to 0$ [27].

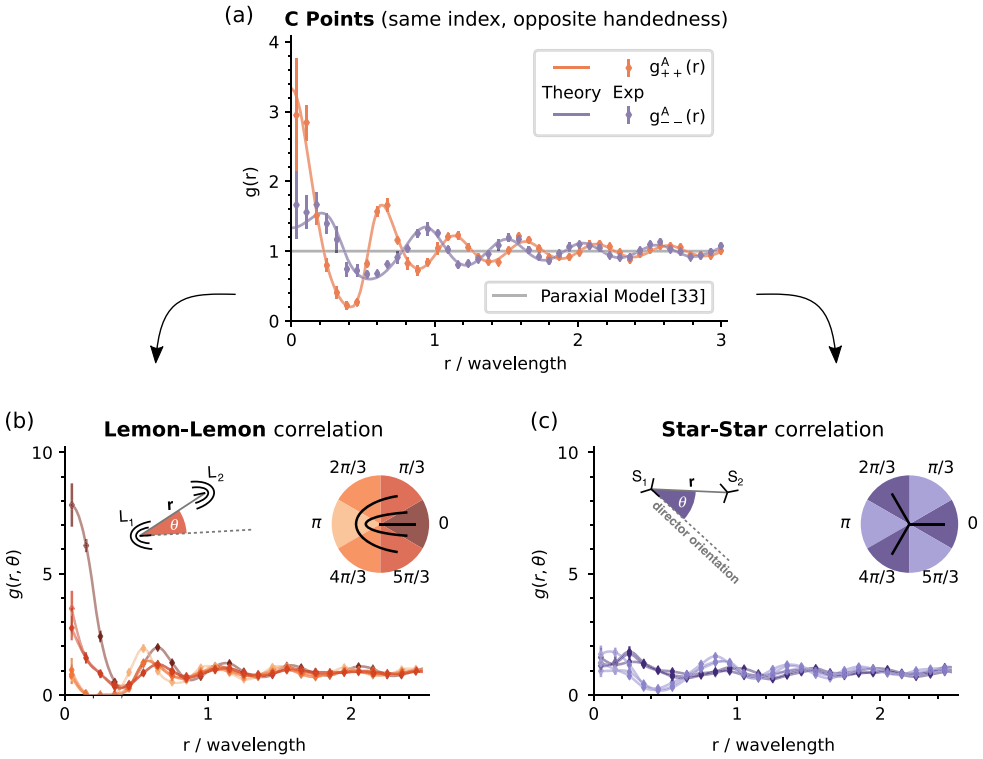

Fig. 4. (a) Pair correlation functions: $g^A_{++}(r)$ for pairs of C points with positive indices (orange) and $g^A_{--}(r)$ for negative pairs (purple). The data points represent the experimental results, while solid lines correspond to the theoretical expectation for polarization singularities in 2D random fields. The gray solid line is the theoretical expectations for C points in a 2D slide of a 3D field, under the paraxial approximation. (b), (c) Pair correlation functions for lemon pairs (b) and star pairs (c) as a function of the displacement angle among the C points, measured with respect to the orientation of one (the) director associated to each singularity (see insets for schematics). In these two plots, the lines are a guide for the eyes.

At distances $r < \lambda/5$, g_{++} is higher than g_{--} by about a factor 2. This preference of two positive index singularities to be in close proximity to each other is consistent with the observation of a larger number of polarization vortices with positive rather than negative index. As the displacement is increased toward values of $r > 2\lambda$ the two correlation functions start to coincide, as they will eventually do for $r \to \infty$, indicating no long-range index-dependent correlations.

From bare intuition there is no reason why a pair of entities with index −1 should behave differently from a pair of index +1. In this regard, it is important to recall that in a 2D slice of a 3D field, C points of opposite handedness would not exhibit any correlation, i.e., $g^A_{++} = g^A_{--} = 1$ [33]. Confining the random field to two dimensions breaks this degeneracy, encouraging pairs of positive C points to approach each other more than negative ones.

We verify this experimental observation by computing the theoretical expectations for the measured pair correlation functions. For the cases of g^A_{++} and g^A_{--} the theoretical curves can be computed with the model described in [27] for a 2D TE random field, with the extra care of treating positive and negative topological indices independently. The pair correlation of polarization vortices requires an extension of the model in [27], since in that framework it corresponds to a higher-order correlation function. In fact, the pair correlation function of polarization vortices can be interpreted as having two same-index C points in $\mathbf{r}_A$ and two in $\mathbf{r}_B$, corresponding to two polarization vortices displaced by $\mathbf{r} = \mathbf{r}_B - \mathbf{r}_A$. In accordance with the notation introduced by Berry and Dennis [20] and also used in [27], such correlation function can be defined as follows:

$$g(\mathbf{r}_B - \mathbf{r}_A) = \frac{\langle \rho[\mathbf{u}_l(\mathbf{r}_A)]\rho[\mathbf{u}_r(\mathbf{r}_A)]\rho[\mathbf{u}_l(\mathbf{r}_B)]\rho[\mathbf{u}_r(\mathbf{r}_B)]\rangle}{\langle \rho[\mathbf{u}_l(\mathbf{r}_A)]\rho[\mathbf{u}_r(\mathbf{r}_A)]\rangle^2}. \quad (2)$$

Here, $\rho[\mathbf{u}_l]$ is the point density of singularities in the left-handed component (ψ_l) of the vector field $\mathbf{E}$ [20,27], i.e.,

$$\rho[\mathbf{u}_l] = \delta(\psi_l')\delta(\psi_l'')\left|\frac{\partial\psi_l'}{\partial x}\frac{\partial\psi_l''}{\partial y} - \frac{\partial\psi_l'}{\partial y}\frac{\partial\psi_l''}{\partial x}\right|, \quad (3)$$

with $\psi_l = \psi_l' + \imath\psi_l''$. For compactness, we use the definition of the vector $\mathbf{u}_l = [\psi_l', \psi_l'', \partial_x\psi_l', \partial_y\psi_l', \partial_x\psi_l'', \partial_y\psi_l'']^\top$ to express the functional dependence on the left-handed field ψ_l and its derivatives. An analogous notation holds for $\mathbf{u}_r$ in relation to the right-handed field ψ_r.

The outcome of the model is plotted as solid lines in Figs. 3 and 4(a). All the essential features of the correlation functions discussed in the previous section are accounted for and no additional ones are revealed. Specifically, the excellent agreement at displacements $r < \lambda/5$ confirms the assessment that the occurring index imbalance of polarization vortices is a result of the 2D confinement of the underlying random field.

C. Topology of the Director Field Around Vortices: Orientation-Dependent Pair Correlation of C Points

Especially with regard to their index-dependent behavior, it is interesting to also consider the line classification of C points. As detailed in [33], the index of C points is related to the topological

properties of the director field around these singularities, with negative index singularities always being star-type, and positive index ones primarily being lemon-type. This line classification is the testament to the broken rotational invariance of the field topology around C points. Thus, we can associate a set of special directions around a C point. These are the directions along which the director of the polarization ellipse points toward the singularity core: three directions for star-type and one for lemon-type [37]. To study director-dependent effects on the spatial correlation of polarization singularities we compute a new set of pair correlation functions, including a dependence on the displacement direction with respect to the C point's directors.

Figures 4(b) and 4(c) present the pair correlation $g(r,\theta)$ of C points as a function of the displacement direction θ with respect to C point directors [see schematics in the insets of Figs. 4(b) and 4(c)]. We restrict the evaluation of $g(r,\theta)$ to the singularities contained in an angular sector of width $\pi/3$ around θ. For lemons (one director), the choice of this reference frame is unambiguous. For stars (three directors), we choose one of their three directors as the reference, at random.

The lemon-lemon correlation function in Fig. 4(b) displays a strong dependence on the displacement angle θ. When approaching $r=0$, the data corresponding to small displacement angles (brown) is approximately 8 times as high as the one corresponding to $\theta \approx \pi$ (light orange). This means that among these closely spaced lemon-lemon pairs, a clear majority is oriented along the direction given by the singularity directors. Quantitatively, among the lemon pairs with displacement $r<\lambda/10$ approximately 50% are aligned within an angle $\pi/6$ with respect to the director of the reference singularity. 35% of the pairs have either orientation $\theta=\pi/3$ or $\theta=5\pi/3$. Finally, the remaining 15% are equally partitioned among $\theta=2\pi/3$, $\theta=\pi$, and $\theta=4\pi/3$. This finding clearly explains the circular pattern of the director field that surrounds positive-index polarization vortices (Fig. 2). For C point separations larger than λ the angular dependence vanishes, and all the correlation functions corresponding to different values of θ start to coincide.

The analysis of the star-star correlation function [Fig. 4(c)] shows a much less clear dependence on the angle θ. Intuitively, given the fact that star-type C points have three directors instead of one, the dependence on θ of their pair correlation $g(r,\theta)$ could be expected to have a periodicity of $2\pi/3$, i.e., to the angle between the three directors of a perfectly symmetric star. We test this hypothesis by computing the correlations $g(r,\theta)$ for $\theta=n\pi/3$ $(n=0,1,\ldots,5)$ and plotting all the functions obtained for even values of n with the same color (dark purple), in contrast to that used for odd values of n (light purple). Figure 4(c) shows that all the pair correlation functions corresponding to angles $\theta'=\theta+2n\pi/3$ are indeed consistent with each other. On the contrary, some difference exists between the functions computed at $\theta_e=2n\pi/3$ and those corresponding to $\theta_o=(2n+1)\pi/3$. This is especially visible in the region $r<\lambda$. The most evident observation here is that $g(r,\theta_o)$ almost vanishes at $r=0.4\lambda$, while $g(r,\theta_e)$ stays close to unity. This indicates that at this particular separation stars tend to stay aligned to the direction of one of their directors rather than avoid it. With respect to the region $r<\lambda/10$, the correlation functions calculated for different values of θ have rather similar values. This is in accordance with topological continuity observations that two stars may join along a common director or pairs of directors can merge together to form a saddle point with four directors [7]. It is important to note that whether a pair of stars would be superimposed while pointing at each other with one of their directors or not, this would still lead to the observed four-pointed star for the director field which surrounds negatively indexed polarization vortices (Fig. 2).

4. LINKING THE INDEX IMBALANCE TO MULTIPOLAR MOMENTS

The influence that the director topology around C points has on their spatial correlations can also be understood qualitatively by linking it to the multipolar moments of the field at the vortex center. We sketch the simplest scenarios of how two lemons or two stars can merge in Fig. 5 [32] and note again that because only the merging of C points with opposite handedness is considered, the resulting higher-order singularity has to have zero in-plane field components. Consequently, the in-plane fields surrounding the singularity lead to, to first order, spatially varying linear polarization, with the direction of the field shown by arrows in Fig. 5. The structure of these local field distributions corresponds to purely longitudinal magnetic and electric dipolar fields for vortices with positive charge as well as fields with only quadrupolar multipole components for negatively charged vortices. This is similar to the fields used in tailored tightly focused light beams to study the multipolar interaction of single nanoparticles [38]. With the random fields under study being purely TE polarized, we can recognize the vanishing correlation $g(0)$ of two merging lemons with anti-aligned directors ($\theta \approx \pi$) as the restriction of a TE mode with no out-of-plane electric field, while the azimuthally oriented polarization structure around the created vortices corresponds to a longitudinal magnetic point dipole m_z at the vortex center. In contrast, positive-index polarization vortices of a TM mode would originate exactly from merging lemon pairs with anti-aligned directors, leading to a longitudinal electric dipole p_z with a radially polarized in-plane electric field structure [13], with the same index imbalance and correlation functions as for TE modes. In addition, the in-plane quadrupolar nature Q_{xy} of the merging of two stars with opposite handedness hints at the lower correlation $g^{A}_{--}(0)$ being a consequence of the need of all six electric and magnetic field components to be zero at this point. Considering the dip in the pair correlation function around $r=\lambda/2$ for two stars with anti-aligned directors, the structure of

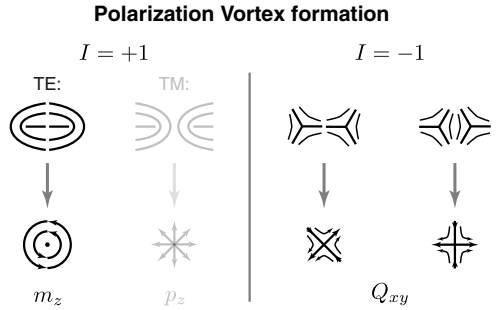

Fig. 5. Sketch of the director orientation around two merging singularities with opposite handedness and same index, leading to dipolar moments p_z and m_z for lemon pairs (left panel, polarization vortex with $I=+1$) and quadrupolar moments Q_{xy} for star pairs (right panel, polarization vortex with $I=-1$).

the two approaching stars suggests an effective repulsion due to the merging of four directors into two.

The restriction to certain field components due to the two-dimensional nature of the field can thus be seen as directly responsible for the resulting index imbalance of polarization vortices, since for an unrestricted 3D field the occurrence of vortices from two C points of opposite handedness would require additionally the concurrence of an L line. This codimension-6 phenomenon [21] of zero field intensity is not expected to occur generically in 3D fields. By reducing the dimension of the field under study, the constraint on the field components is lifted for polarization vortices with positive index, leading to the observed positive index imbalance of the charge correlation function $g_I(r)$.

In addition, this restriction to certain multipolar moments of the field at polarization vortices implies that as soon as a certain level of (experimentally unavoidable) noise is introduced to any tailored 2D field, the allowed light–matter interaction of the field with a small probe (be it a molecule, quantum dot, or scattering particle) will be governed at high symmetry points only by the shown multipolar moments.

5. CONCLUSION

In this paper we presented the experimental observation of higher-order singularities of the polarization state of a random light field, known as polarization vortices. We discovered that polarization vortices in random waves exhibit a clear spatial correlation, with measured values for their pair correlation function reaching values larger than 4. Most interestingly, we saw an imbalance in the total topological index of the detected vortices: more than twice as many positive vortices were observed as negative ones. We traced back this observation to the fact that C points with positive index are more often found at vanishing mutual distances than negative ones. Moreover, we found that at short distances, positive C points (mostly lemons) prefer to align along the direction of the director of the singularity, while negative C points (stars) do not exhibit a clear preferential direction. These observations find their explanation in the fact that a truly 2D (TE) random field is investigated, as no index imbalance is to be expected for a 2D slice of a 3D field. In fact, the model developed in [27] for 2D random fields describes our experimental findings in great detail. It is important to stress that the lower dimensionality and the resulting correlations among the vector field components is the true cause of the observations made in this paper, which could inspire the development of a more universal description of the behavior of C points. Finally, we note that these results are quite general for the 2D case, as they apply to both TE and TM in-plane fields.

APPENDIX A: DETECTION OF POLARIZATION VORTICES

To experimentally determine polarization vortices, some modifications to the generic algorithm for detecting singularities in complex scalar fields on a rectangular grid are necessary. We call to mind that C points (index $\pm 1/2$) are phase singularities (charge ± 1) in the constructed complex Poincaré field $\Psi = S_1 + iS_2$ [39], where S_1 and S_2 are the first and second Stokes parameter, respectively. Therefore, polarization vortices (index ± 1) appear as phase vortices of charge ± 2 in Ψ. In order to determine the location of polarization vortices, we need to be able to detect a phase circulation of $\pm 4\pi$. Such a phase change is too fast to be encoded in 2×2 pixels. The generic algorithm of finite difference phase loops will always indicate the existence of a pair of single-order singularities displaced by a single pixel. At this point two approaches can be pursued. In a first approach one can establish the criterion for which two C points displaced by a single pixel correspond to a single polarization vortex. Alternatively, a new detection algorithm can be designed to perform phase integrals over 3×3 pixel loops. This larger integration path allows for the direct visualization of second-order singularities. After verifying that both approaches yield the same result, we only applied the second method for the data presented in this paper.

APPENDIX B: INDEX IMBALANCE AND CHARGE CORRELATION FUNCTION

If more polarization vortices with positive than negative index are present in a random light field, the number of same-sign vortex pairs will by necessity always be higher than that of opposite-signed pairs, yielding a positive value of the charge correlation function g_I at large distances. In more detail, having N_+ positive vortices and N_- negative ones, with $N_+ = fN_-$, results in N_{same} pairs of same-charge singularities,

$$\begin{aligned} N_{\text{same}} &= N_+(N_+ - 1) + N_-(N_- - 1) \\ &= (1 + f^2)N_+^2 + o(N_+), \end{aligned} \tag{B1}$$

and N_{opp} with opposite charges,

$$N_{\text{opp}} = N_+N_- + N_-N_+ = 2fN_+^2. \tag{B2}$$

When $r \to \infty$, we can neglect the term $o(N_+)$, so

$$\begin{aligned} g_I(r \to \infty) &\propto N_{\text{same}} - N_{\text{opp}} \propto 1 + f^2 - 2f \\ &= (1 - f)^2 > 0 \quad \forall\, f \neq 1. \end{aligned} \tag{B3}$$

Funding. Nederlandse Organisatie voor Wetenschappelijk Onderzoek; FP7 Ideas: European Research Council (340438); H2020 Marie Skłodowska-Curie Actions (748950).

Acknowledgment. We thank Andrea Di Falco for fabricating the chaotic cavity used in the near-field experiments.

REFERENCES

1. H. Riehl, "A model of hurricane formation," J. Appl. Phys. **21**, 917–925 (1950).
2. LIGO Scientific Collaboration and Virgo Collaboration, "Observation of gravitational waves from a binary black hole merger," Phys. Rev. Lett. **116**, 061102 (2016).
3. A. K. Spilman and T. G. Brown, "Stress birefringent, space-variant wave plates for vortex illumination," Appl. Opt. **46**, 61–66 (2007).
4. B. Zhen, C. W. Hsu, L. Lu, A. D. Stone, and M. Soljačić, "Topological nature of optical bound states in the continuum," Phys. Rev. Lett. **113**, 257401 (2014).
5. Y. Zhang, A. Chen, W. Liu, C. W. Hsu, B. Wang, F. Guan, X. Liu, L. Shi, L. Lu, and J. Zi, "Observation of polarization vortices in momentum space," Phys. Rev. Lett. **120**, 186103 (2018).
6. H. M. Doeleman, F. Monticone, W. Hollander, A. Alù, and A. F. Koenderink, "Experimental observation of a polarization vortex at an optical bound state in the continuum," Nat. Photonics **12**, 397–401 (2018).
7. G. J. Gbur, *Singular Optics* (CRC Press, 2016).
8. K. Volke-Sepulveda, V. Garcés-Chávez, S. Chávez-Cerda, J. Arlt, and K. Dholakia, "Orbital angular momentum of a high-order Bessel light beam," J. Opt. B **4**, S82–S89 (2002).

9. S. N. Alperin and M. E. Siemens, "Angular momentum of topologically structured darkness," Phys. Rev. Lett. **119**, 203902 (2017).
10. G. Milione, H. I. Sztul, D. A. Nolan, and R. R. Alfano, "Higher-order Poincaré sphere, Stokes parameters, and the angular momentum of light," Phys. Rev. Lett. **107**, 053601 (2011).
11. L. Dominici, G. Dagvadorj, J. M. Fellows, D. Ballarini, M. De Giorgi, F. M. Marchetti, B. Piccirillo, L. Marrucci, A. Bramati, G. Gigli, M. H. Szymańska, and D. Sanvitto, "Vortex and half-vortex dynamics in a nonlinear spinor quantum fluid," Sci. Adv. **1**, E1500807 (2015).
12. E. Otte, C. Alpmann, and C. Denz, "Higher-order polarization singularities in tailored vector beams," J. Opt. **18**, 074012 (2016).
13. S. Quabis, R. Dorn, M. Eberler, O. Glöckl, and G. Leuchs, "Focusing light to a tighter spot," Opt. Commun. **179**, 1–7 (2000).
14. C. Maurer, A. Jesacher, S. Fürhapter, S. Bernet, and M. Ritsch-Marte, "Tailoring of arbitrary optical vector beams," New J. Phys. **9**, 78 (2007).
15. Q. Zhan, "Cylindrical vector beams: from mathematical concepts to applications," Adv. Opt. Photonics **1**, 1–57 (2009).
16. F. Cardano, E. Karimi, S. Slussarenko, L. Marrucci, C. de Lisio, and E. Santamato, "Polarization pattern of vector vortex beams generated by q-plates with different topological charges," Appl. Opt. **51**, C1–C6 (2012).
17. M. Neugebauer, T. Bauer, A. Aiello, and P. Banzer, "Measuring the transverse spin density of light," Phys. Rev. Lett. **114**, 063901 (2015).
18. D. Naidoo, F. S. Roux, A. Dudley, I. Litvin, B. Piccirillo, L. Marrucci, and A. Forbes, "Controlled generation of higher-order Poincaré sphere beams from a laser," Nat. Photonics **10**, 327–332 (2016).
19. H. Rubinsztein-Dunlop, A. Forbes, M. V. Berry, M. R. Dennis, D. L. Andrews, M. Mansuripur, C. Denz, C. Alpmann, P. Banzer, T. Bauer, E. Karimi, L. Marrucci, M. Padgett, M. Ritsch-Marte, N. M. Litchinitser, N. P. Bigelow, C. Rosales-Guzmán, A. Belmonte, J. P. Torres, T. W. Neely, M. Baker, R. Gordon, A. B. Stilgoe, J. Romero, A. G. White, R. Fickler, A. E. Willner, G. Xie, B. McMorran, and A. M. Weiner, "Roadmap on structured light," J. Opt. **19**, 013001 (2017).
20. M. V. Berry and M. R. Dennis, "Phase singularities in isotropic random waves," Proc. R. Soc. London A **456**, 2059–2079 (2000).
21. M. V. Berry and M. R. Dennis, "Polarization singularities in isotropic random vector waves," Proc. R. Soc. London A **457**, 141–155 (2001).
22. F. Flossmann, U. T. Schwarz, M. Maier, and M. R. Dennis, "Polarization singularities from unfolding an optical vortex through a birefringent crystal," Phys. Rev. Lett. **95**, 253901 (2005).
23. N. Shvartsman and I. Freund, "Vortices in random wave fields: Nearest neighbor anticorrelations," Phys. Rev. Lett. **72**, 1008–1011 (1994).
24. I. Freund and N. Shvartsman, "Wave-field phase singularities: The sign principle," Phys. Rev. A **50**, 5164–5172 (1994).
25. L. De Angelis, F. Alpeggiani, A. Di Falco, and L. Kuipers, "Spatial distribution of phase singularities in optical random vector waves," Phys. Rev. Lett. **117**, 093901 (2016).
26. L. De Angelis and L. Kuipers, "Screening and fluctuation of the topological charge in random wave fields," Opt. Lett. **43**, 2740–2743 (2018).
27. L. De Angelis, F. Alpeggiani, and L. Kuipers, "Spatial bunching of same-index polarization singularities in two-dimensional random vector waves," Phys. Rev. X **8**, 041012 (2018).
28. M. Burresi, R. J. P. Engelen, A. Opheij, D. van Oosten, D. Mori, T. Baba, and L. Kuipers, "Observation of polarization singularities at the nanoscale," Phys. Rev. Lett. **102**, 033902 (2009).
29. L. De Angelis, F. Alpeggiani, A. Di Falco, and L. Kuipers, "Persistence and lifelong fidelity of phase singularities in optical random waves," Phys. Rev. Lett. **119**, 203903 (2017).
30. B. Le Feber, N. Rotenberg, D. M. Beggs, and L. Kuipers, "Simultaneous measurement of nanoscale electric and magnetic optical fields," Nat. Photonics **8**, 43–46 (2014).
31. J. F. Nye, "Lines of circular polarization in electromagnetic wave fields," Proc. R. Soc. London A **389**, 279–290 (1983).
32. T. Delmarcelle and L. Hesselink, "The topology of symmetric, second-order tensor fields," in *Proceedings of the IEEE Conference on Visualization* (1994), Vol. **1**, pp. 140–147.
33. M. R. Dennis, "Polarization singularities in paraxial vector fields: morphology and statistics," Opt. Commun. **213**, 201–221 (2002).
34. M. R. Dennis, "Polarization singularity anisotropy: determining monstardom," Opt. Lett. **33**, 2572–2574 (2008).
35. J. A. Barker and D. Henderson, "What is 'liquid'? understanding the states of matter," Rev. Mod. Phys. **48**, 587–671 (1976).
36. G. Miller, B. Nefkens, and I. Šlaus, "Charge symmetry, quarks and mesons," Phys. Rep. **194**, 1–116 (1990).
37. M. V. Berry, "Regular and irregular semiclassical wavefunctions," J. Phys. A **10**, 2083–2091 (1977).
38. P. Woźniak, P. Banzer, and G. Leuchs, "Selective switching of individual multipole resonances in single dielectric nanoparticles," Laser Photonics Rev. **9**, 231–240 (2015).
39. I. Freund, "Poincaré vortices," Opt. Lett. **26**, 1996–1998 (2001).